Journal of Nuclear Materials 390–391 (2009) 814–817

Contents lists available at ScienceDirect

Journal of Nuclear Materials

journal homepage: www.elsevier.com/locate/jnucmat

Experimental study of plasma energy transfer and material erosion under ELM-like heat loads

I.E. Garkusha [a,*], V.A. Makhlaj [a], V.V. Chebotarev [a], I. Landman [b], V.I. Tereshin [a], N.N. Aksenov [a], A.N. Bandura [a]

[a] Institute of Plasma Physics of the NSC KIPT, Akademicheskaya 1, 61108 Kharkov, Ukraine
[b] Forschungszentrum Karlsruhe, IHM, 76021 Karlsruhe, Germany

ARTICLE INFO

PACS:
52.40.Hf

ABSTRACT

Main features of plasma–surface interaction and energy transfer to tokamak plasma facing components are studied at different heat loads in ELM simulation experiments with the plasma gun QSPA Kh-50. Repetitive plasma exposures of tungsten, graphite and different combined W-C targets were performed at the pulse duration of 0.25 ms and the heat loads varied in the range 0.2–2.5 MJ/m^2. The onset of vapor shield in front of the surface was investigated. The evaporation is immediately followed by a saturation of surface heat load if further increasing the impact energy. The presence of graphite essentially decreases the heat flux to the nearby tungsten surface, which is due to the carbon vapor shield. Droplet splashing at the tungsten surface and formation of hot spots on the graphite surface are discussed.

1. Introduction

Experimental investigations of plasma–surface interaction (PSI) in the conditions simulating transient events in the fusion reactor ITER are important for determination of erosion mechanisms of plasma facing materials as well as the dynamics of erosion products, the impurities transport in the plasma, and the influence of vapor shield on the plasma energy transfer to material surface. The obtained results can be used for validation of predictive numerical models for ITER and DEMO developed for estimations of tolerable size of Type I ELMs and lifetime of divertor armour materials.

As it was shown earlier in disruption simulation experiments with plasma guns [1,2] and in numerical modeling [3,4], the main feature of high-power plasma interaction with material surfaces is formation of a dense plasma shield in front of the target. Due to the strong shielding at the disruption-like loads of 10–20 MJ/m^2 only several percents of plasma energy reach the surface [1,2]. It should be mentioned that in the disruption simulation experiments the dense vapor shield was studied mainly for graphite and CFC targets. For the possible ITER ELMs impacting on the tungsten surface, the shielding layer properties have yet to be investigated especially for the plasma loads which are very close to the evaporation threshold.

Energy densities deposited during ELMs are much less than that of disruptions. The ELM heat loads in ITER are expected to be up to $Q < 3$ MJ/m^2 during $\tau = (0.1 \ldots 0.5)$ ms [5]. However, some shielding can also appear in this case. Onset of vapor shield and effects of 'weak' shielding for a single ELM may contribute significantly to the resulting surface damage due to expected large number (up to 10^6) of repetitive ELMs.

In the first period of ITER operation both tungsten and CFC as adjoin materials for divertor components which are able to withstand the transient high-heat loads are foreseen [5]. The PSI issues following from the neighborhood of tungsten and carbon on the divertor plate surfaces can be analyzed comprehensively using plasma guns, as from the point of redeposition and chemical reactions (carbides etc.) as the characteristics of adjoined W and C area, in the conditions simulating the transient events, like ELMs.

This paper presents the results of plasma gun experiments on high-power interactions with material surfaces under the conditions typical for ITER Type I ELMs. The experiments include the measurements of plasma energy deposited in the material surface as a function of the impact energy and thus the onset energy of vapor shield for W, C and adjoined W-C surfaces under repetitive ELM relevant plasma exposures.

2. Experimental setup

The samples have been exposed to hydrogen plasma streams produced by the quasi-steady-state plasma accelerator QSPA Kh-50, described elsewhere [6–8]. Scheme of plasma exposures is presented in Fig. 1. QSPA Kh-50 consists of two stages. The first one is used for plasma production and pre-acceleration. The main second

* Corresponding author.
E-mail address: garkusha@ipp.kharkov.ua (I.E. Garkusha).

0022-3115/$ - see front matter © 2009 Elsevier B.V. All rights reserved.
doi:10.1016/j.jnucmat.2009.01.215

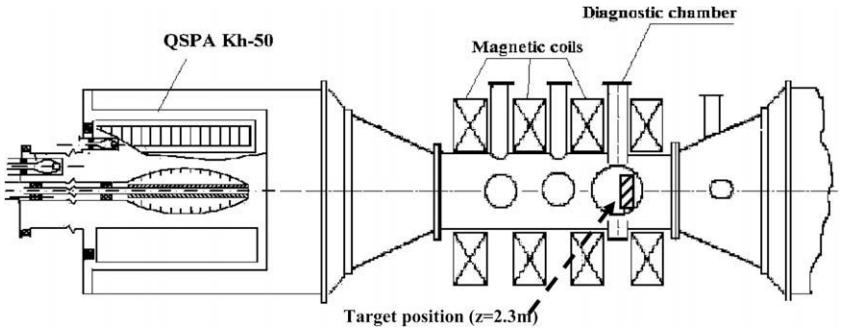

Fig. 1. Scheme of targets exposures.

stage is a coaxial system of shaped active electrodes with magnetically screened elements, supplied from independent power sources. The plasma streams, generated by QSPA Kh-50, are injected into the magnetic system of 1.6 m in length and 0.44 m in inner diameter with a magnetic field of up to 0.54 T in diagnostic chamber where the target has been installed (Fig. 1).

The experiments were performed with repetitive pulses of the duration of 0.25 ms and the heat loads in the range of 0.2–2.5 MJ/m^2, which simulate the ELMs impact in ITER. The plasma stream diameter is 18 cm, the ion energy is about 0.4 keV, and maximum plasma pressure achieves 3.2 bar.

Interferometry, spectroscopy, piezo-detectors, electric and magnetic probes, and other diagnostics were applied for measurements of plasma stream parameters in different regimes of operation. The diagnostics are described in more details elsewhere [1,8,11]. Radial distributions of the plasma stream energy density were monitored with movable thermocouple calorimeters at the different distances from plasma gun. Plasma stream power and energy densities were also calculated on the basis of measurements of the time dependencies of the plasma pressure, plasma stream density and its velocity.

The energy density absorbed by the target was measured with small thermocouple calorimeters inserted into surface layer of W and C targets [1,9]. Observations of plasma interactions with exposed surfaces and droplets monitoring were performed with high-speed CMOS camera PCO AG.

3. Experimental results

Fig. 2 shows the heat load to the tungsten, graphite and combined W-C target surfaces, which was measured with calorimetry, in dependence on energy density of impacting plasma stream. For tungsten target exposure onset of melting is observed on the surface at surface heat load of 0.57 MJ/m^2. The measurements demonstrate that even for plasma exposures, which not result in the melting, the absorbed heat load is about 55–60% of the impact plasma energy. The dynamical screening of the surface from impacting plasma stream appears in this case probably due to the shock wave formation and plasma stream thermalization under the interaction with target surface. The stopped plasma layer, formed from the head of the plasma stream, ceases to be completely transparent for subsequently impacting plasma ions. Tungsten vapor shield formation and its influence on plasma energy transfer to the surface become clearly seen as the surface heat load achieves 1.1 MJ/m^2. The fraction of plasma energy, which is absorbed by the target surface, is rapidly decreased with achieving the evaporation onset for exposed targets. At this, the value of heat load to the surface remains practically constant with further increase of the energy density of impacting plasma (plateau region in Fig. 2).

The evaporation leads to enhanced mass losses of tungsten: increase of the heat load from 0.75 to 1.1 MJ/m^2 raises mass losses for one order of magnitude and causes bubble structures at the surface. Due to achievement of evaporation threshold, the erosion crater become visible even on the 'background' of the surface roughness and swelling. The erosion rate caused by evaporation is ~0.05 μm/pulse. Microscopy observations of tungsten targets show boiling bubbles on the surface exposed with heat load of 1.1 MJ/m^2 (Fig. 3). For initial pulses the boiling is initiated on the surface by impurities. With further exposures it becomes predominantly volumetric and deep bubbles are arisen at the surface. The volumetric boiling occurs predominantly at the vicinity of crack edges.

Measurements of the energy transfer for combined tungsten–graphite targets of different sizes demonstrate that the value of energy density delivered to the target surface is reduced in comparison with tungsten irradiation (Fig. 2). Carbon neighborhood resulted in the shielding which develops for lower heat loads. Experiments with MPG-7 graphite targets show that carbon evaporation starts at 0.4–0.45 MJ/m^2. Carbon vapor shield formation during exposures of combined W-C targets results in additional decrease of the heat loads to W surface (from 1.1 MJ/m^2 to 0.8 ... 0.85 MJ/m^2) preventing tungsten evaporation. It should be noted that tungsten evaporation threshold in the case of adjoined graphite surface was not achieved even with increasing plasma stream energy density (Fig. 2).

Plasma impacts with loads above the melting threshold cause the droplets splashing from the tungsten surface. As an example, Fig 4(a) and (b) shows images of the droplets traces for 2 time moments after plasma pulse. The applied measurement scheme for droplets monitoring was similar to used in [9,10]. Exposition time for each image is 1.2 ms and the velocity of the droplets can be estimated from the lengths of their traces. Movement in perpendicular direction to the image plane is derived from consecutive

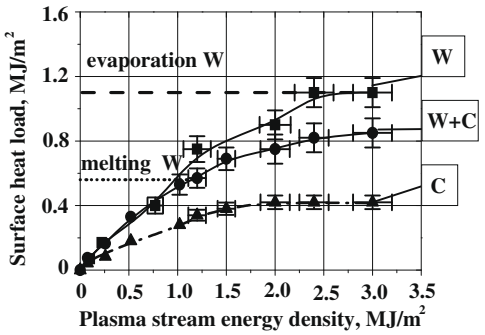

Fig. 2. Heat load to the target surfaces vs. the energy density of impacting plasma stream.

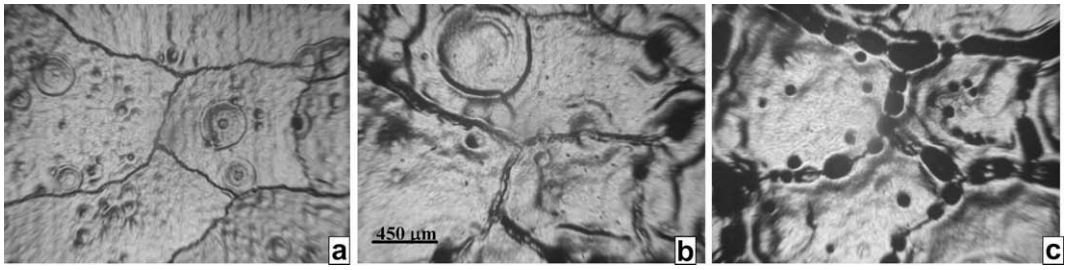

Fig. 3. Boiling bubbles on the tungsten surface exposed with 5 (a), 25 (b) and 80 (c) pulses of 1.1 MJ/m^2 (the same surface region).

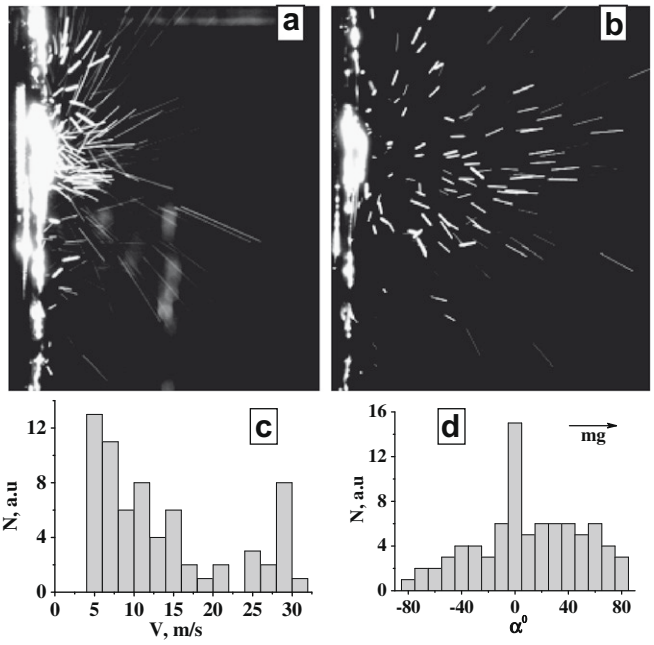

Fig. 4. Droplets splashing from W melt. Images of droplet traces $t_{exposure}$ = 1.2 ms, t = 3.0 ms after plasma pulse (a), t = 9.0 ms (b), velocity (c) and angular (d) distributions of ejected droplets for t = 3.0 ms.

frames. Consequences of the images form movie with possibility to analyze the dynamics of droplets splashing from the surface.

Droplets continue to be ejected from the melt after plasma impact during >10 ms. Tungsten cracking causing decrease of the heat transfer between the melt layer and a cold bulk, as well as the vapor shied formation in front of the surface, may influence significantly on the resolidification time and, thus, on the measured duration of droplets splashing. It is obtained that droplets velocities may achieve several tens m/s. Fast droplets are generated at earlier time moments. Smaller velocities are observed for late stage of observation (Fig. 4(b)). During intermediate stage both groups of droplets with fast and lower velocities are observed (Fig. 4(a) and (c)).

Angular distribution of ejected droplets is presented in Fig. 4(d). For perpendicular to the surface plasma impacts droplets are ejected primarily with small angles to the normal. Nevertheless rather large angles up to 80° are measured also. Analysis of droplet traces from consecutive images show the influence of gravitational force for droplets with higher mass and smaller velocities. Due to the gravitation the resulting angular distribution of the droplets became non-symmetric (Fig. 4(d)). With achieving evaporation threshold the tungsten boiling results in intensification of the droplets splashing. Their size is varied in the range of (5–100) μm.

Dynamics of tungsten and carbon vapor in front of the targets surfaces, which was studied with spectroscopy and high-speed photography during the plasma pulse, and it dependence on the magnitude of external magnetic field is described in [8]. Here it can be only mentioned that evaporated tungsten is concentrated in rather thin plasma layer of <0.5 cm close to the surface and it does not propagate significantly in upstream direction during the QSPA pulse. In the case of graphite target exposure, high-speed photography shows continuous region of carbon vapor luminosity. Thickness of the shielding layer increases during the pulse and exceeds 5 cm. Spectroscopy measurements demonstrate that carbon lines are registered not only in front of the target surface, but also for larger distances (at least, up to 20 cm) from the target.

Fig. 5 shows the hot spots indicating overheated local areas on the graphite surface of combined W-C target (tungsten rod of 1 cm diameter surrounded by MPG-7 graphite of 8 cm in diameter). The target was subjected to inclined plasma impact $\alpha = 45°$. Surface heat load Q_{surf} = 0.5 MJ/m^2. The images correspond to t_{start} = 0.7 ms and t_{start} = 3.7 ms after plasma pulse respectively. Exposition time of each image is t_{exp} = 0.5 ms. It should be noted much more pronounced heating of upstream part of the inclined target edge, which is demonstrated by Fig. 5. This is valid also for tungsten rod in target center (Fig. 5(a)).

Hot spots of are formed on graphite surface probably due to surface relief developed. The heat load to the inclined target surface (0.5 MJ/m^2) is below the melting threshold of tungsten. Thus the

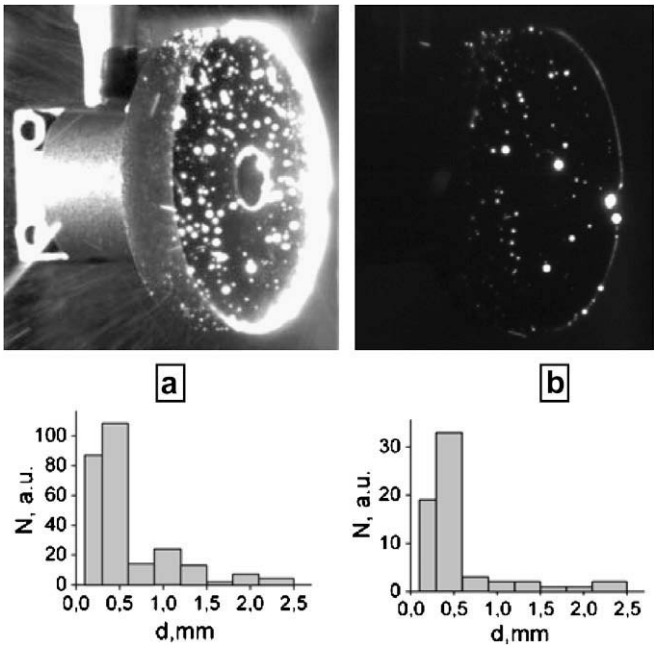

Fig. 5. Images and size distributions of hot spots on graphite surface of combined W-C target (tungsten rod of 1 cm diameter surrounded by MPG-7 graphite of 8 cm in diameter) indicating overheated areas. Inclined impact = 45°, t_{exp} = 0.5 ms, t = 0.7 ms (a), t = 3.7 ms (b), Q_{surf} = 0. 5 MJ/m^2.

observed bright spots are not caused by W droplets. Corresponding high-speed imaging proved that this luminosity can not also be attributed to carbon dust, which could be redeposited back to the surface in the end on plasma pulse. Hot spots indicate the areas of enhanced evaporation and their luminosity is observed during ~30 ms after plasma impact. Size distributions of the hot spots are also presented in Fig. 4 for time moments of each image. It was impossible to perform analysis of micro-spots with larger magnification while the target is in vacuum chamber. Nevertheless, most of registered spots are ~0.1–0.5 mm in diameter, which is much larger than maximal size of the grains in MPG-7 graphite (10–25 m). Qualitatively the size distribution of the spots remains similar for different time moments after the end of pulse. The only number of overheated areas is decreased and luminosity of some spots disappears with time.

4. Conclusions

The energy transfer to tungsten and graphite material surfaces was studied in ITER ELM simulation experiments with the plasma gun QSPA Kh-50. The plasma exposures of W, C, and W-C targets were performed with repetitive pulses of the duration 0.25 ms and the heat loads varied in the range 0.2–2.5 MJ/m^2.

The onset of vapor shield formation in front of the surface under ELM-like plasma loads was studied. Achievement of evaporation threshold for exposed targets results in further saturation of heat load absorbed by the surface if continue increasing impact energy density. For tungsten targets the vapor shield and its influence on energy transfer to the surface become significant when the surface heat load exceeds 1.1 MJ/m^2. The evaporation results in enhanced mass loss and formation of erosion crater and large bubbles on the surface.

The influence of carbon PFCs on the plasma energy transfer to nearby tungsten surfaces is demonstrated. The carbon protects the tungsten surface at lower heat loads than are needed for tungsten vaporization: graphite starts to evaporate at 0.4–0.45 MJ/m^2 and the carbon vapor shield screens the heat loads to W surface above 0.8 ... 0.85 MJ/m^2 thus completely preventing tungsten evaporation.

After the exposures of isotropic fine grain graphite MPG-7, high-speed imaging shows some non-uniform surface heating and overheated areas even. The hot spots of the sizes 0.1–0.5 mm which indicate the areas of enhanced evaporation are formed on graphite surface probably due to the surface relief development after multiple irradiations. The hot spot luminosity is observed during ~30 ms after plasma impact.

The plasma impacts cause the droplet splashing from the tungsten surface. Angular distribution of splashed droplets was analyzed. The W-droplets continue to be ejected from the melt for about 10 ms after the impact. The droplets velocities may achieve several tens m/s. Fast droplets are generated at earlier time moments, and small droplet velocities correspond to the late stage of observation.

Acknowledgements

This work has been supported in part by STCU Project #4155. The authors would like to acknowledge N.V. Kulik, V.V. Staltsov, S.I. Lebedev and P.V. Shevchuk for assisting in the experiments.

References

[1] V.V. Chebotarev et al., J. Nucl. Mater. 233–237 (1996) 736.
[2] N. Arkhipov et al., Fus. Technol. 32 (1997) 45.
[3] H. Würz et al., J. Nucl. Mater. 220–222 (1995) 1066.
[4] A. Hassanein, I. Konkashbaev, J. Nucl. Mater. 233–237 (1996) 713.
[5] G. Federici et al., Plasma Phys. Control. Fus. 45 (2003) 1523.
[6] I.E. Garkusha et al., J. Nucl. Mater. 363–365 (2007) 1021.
[7] V.A. Makhlaj et al., Phys. Scr. T128 (2007) 111.
[8] V.I. Tereshin et al., Plasma Phys. Control. Fus. 49 (2007) A231.
[9] A. Zhitlukhin et al., J. Nucl. Mater. 363–365 (2007) 301.
[10] J. Linke et al., Phys. Scr. T91 (2001) 36.
[11] A.N. Bandura et al., Phys. Scr. 123 (2006) 84.